Effects of Laser Energy on Zinc Oxide Thin Films Prepared by Pulsed Laser Deposition for Solar Cells

1st Ahmed S. Jaber
Information and Communication Technology Research Center
Scientific Research Commission, Baghdad, Iraq
ahmedcctv11@gmail.com

2nd Khalil I. Inad
Information and Communication Technology Research Center,
Scientific Research Commission, Baghdad, Iraq
dr.khalil.inad@gmail.com

3rd Sawsan H. Abdullah*
Information and Communication Technology Research Center,
Scientific Research Commission, Baghdad, Iraq
sawsanhussein1976@gmail.com

*Corresponding author: sawanhussein1976@gmail.com.

Received: 2026-07-02; **Accepted:** 2026-08-10

***Abstract*—Zinc oxide thin films were deposited using pulsed laser deposition at 400, 500, and 600 millijoules. X-ray diffraction showed polycrystalline hexagonal wurtzite structures oriented along the 002 direction. Crystallite sizes ranged from 21.3 to 33.7 nanometers depending on laser energy. Atomic force microscopy revealed grain size increased from 52 to 85 nanometers at higher energies, while average surface roughness decreased from 3.6 to 1.3 nanometers. This indicates smoother, more uniform surfaces. Scanning electron microscopy confirmed improved surface homogeneity and reduced aggregation at 600 millijoules. Optically, raising laser energy increased transmittance and widened the bandgap from 2.65 to 3.19 electron volts. Films deposited at 600 millijoules achieved 92.8 percent optical transmittance at 950 nanometers. Furthermore, higher laser power significantly enhanced zinc oxide and porous silicon solar cell performance. The open-circuit voltage increased to 0.36 volts, and short-circuit current density reached 23 milliamperes per square centimeter. Maximum output power grew from 2.08 to 2.99 milliwatts per square centimeter, boosting conversion efficiency from 2.08 to 2.99 percent. Ultimately, increasing deposition energy from 400 to 600 millijoules critically improves the structural, morphological, optical, and photovoltaic properties of zinc oxide thin films for advanced solar applications.**

***Keywords*—zinc oxide, pulsed laser deposition, x-ray diffraction, atomic force microscopy.**

I. INTRODUCTION

Semiconductors are important in numerous technological applications, from electronic applications (e.g., photovoltaic systems, sensors, etc.) to medical and biological applications [1]–[4]. Zinc oxide (ZnO) is a Group II-VI semiconductor with a wide band gap, with a direct transition energy of ~ 3.3 eV and a high exciton binding energy of ~ 60 meV [5]. Zinc oxide is non-toxic, naturally occurring, and inexpensive [6]. This makes zinc oxide a good choice for solar cell applications as a transparent conductive oxide, serving as a very practical substitute for indium and tin oxides. Its cost-effectiveness and good physical properties make it suitable for use as a window layer [7], [8]. Zinc oxide films have been produced from vacuum thermal evaporation [9], spray deposition [10], chemical deposition [11], laser ablation [12], and plasma jetting [13].

One of the methods adopted for the production of zinc oxide thin films is pulsed laser deposition (PLD) [14], which enables the formation of high-purity films while retaining control over thickness and stoichiometry [15]–[17]. Moreover, PLD allows precise control of film properties by varying deposition parameters, especially laser energy [18], [19]. The optical and electrical properties of PLD-produced zinc oxide films are particularly attractive for solar cells due to increased device efficiency [20]. Although various studies have investigated the effects of deposition parameters on zinc oxide characteristics [21]–[23], a systematic comparison focusing on structural, morphological, and optical properties across various laser energies—along with their integration into photovoltaic devices—remains highly valuable. Therefore, this study investigates the effects of PLD laser energy (400, 500, and 600 mJ) on the structural, morphological, and optical properties of zinc oxide films. Furthermore, zinc oxide films are deposited onto porous silicon (PSi) to form photovoltaic structures, evaluating how laser-induced modifications of the zinc oxide films influence overall device performance.

II. EXPERIMENTAL PART

The Neodymium-doped Yttrium Aluminum Garnet (Nd:YAG) laser system used operates at a wavelength of 1064 nm, with pulse energy values covering the range of 100 to 1000 mJ, a pulse duration of 5 to 10 ns, a repetition frequency between 1 and 10 Hz, a beam diameter ranging from 3 to 8 mm, and an energy fluence ranging from 1 to 5 J/cm² depending on the specific settings utilized. For this study, the deposition using the Nd:YAG laser was conducted at energy levels of 400 to 600 mJ with a peak pulse duration of approximately 9 ns, a repetition frequency of 6 Hz, and 200 laser shots. Zinc oxide deposition took place at room temperature onto glass substrates. Laser beam deposition was carried out within a vacuum chamber at a base pressure of 2.5×10^{-2} mbar. The substrate holders were accurately positioned within the chamber to match the laser beam path. The focused Nd:YAG laser beam entered through an optical window and struck the target surface at a 45° angle. The substrate was placed directly in front of the target with its surface parallel to the target face, maintaining adequate spacing to prevent the substrate holder from obstructing the incoming laser beam. The methodological approach of the pulsed laser deposition system is illustrated in Fig. 1. Detailed experimental parameters for zinc oxide thin-film deposition and porous silicon fabrication are summarized in Table I and Table II, respectively.

III. RESULTS AND DISCUSSION

Fig. 2 illustrates the X-ray diffraction patterns of zinc oxide thin films synthesized using the pulsed laser deposition method across a range of laser energy levels (400, 500, and 600 mJ). The diffraction patterns reveal distinct peaks at 2θ

Vol. 08 No. 2, October-2026, Pages 65-70 DOI: https://dx.doi.org/10.20961/jeeict.8.2.122974

positions close to 31.5°, 34.1°, 36.0°, 56.4°, 62.8°, and 67.8°, which correspond to the (100), (002), (101), (110), (103), and (112) crystallographic planes. These peaks match the hexagonal wurtzite structure of zinc oxide in agreement with ICDD card No. 96-901-1663, confirming the successful growth of crystalline zinc oxide thin films [24]–[26]

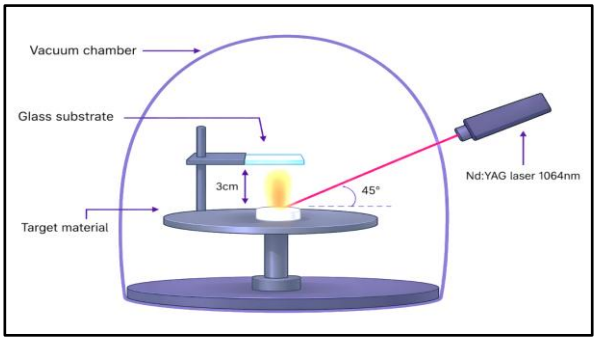

Fig. 1. Diagram for Pulse Laser Deposition technique.

TABLE I. EXPERIMENTAL PARAMETERS USED FOR ZNO THIN-FILM DEPOSITION

Parameter	Value
Laser wavelength	1064 nm
Laser energy	400, 500, 600 mJ
Pulse duration	9 ns
Repetition rate	6 Hz
Number of laser pulses	200 shots
Laser spot diameter	1 mm
Laser fluence at 400 mJ	50.9 J/cm²
Laser fluence at 500 mJ	63.7 J/cm²
Laser fluence at 600 mJ	76.4 J/cm²
ZnO target purity	99.9%
Target cleaning	Ultrasonic cleaning
Target-to-substrate distance	3 cm
Substrate temperature	Room temperature
Chamber pressure	2.5×10^{-2} mbar
Film thickness	~200 nm
Thickness measurement	Optical interferometer
Thickness measurement laser	He–Ne laser
He–Ne wavelength	632.8 nm
XRD instrument	Bruker D2 PHASER
XRD radiation	Cu-Kα (λ = 1.5406 Å)
AFM instrument	CSPM-AA3000 (Digital Instruments)
AFM operating mode	Non-contact mode
SEM instrument	Thermo Scientific SEM

TABLE II. PSI FABRICATION AND ZNO/PSI PHOTOVOLTAIC DEVICE PARAMETERS

Parameter	Value
PSi fabrication technique	Photo Electrochemical Etching (PECE)
PECE cell material	Teflon
Exposed silicon area	1 cm²
Bottom electrode	Stainless-steel disk
Counter electrode	Platinum mesh
Electrolyte	HF + ethanol
HF:ethanol ratio	2:1
Etching current density	50 mA/cm²
Etching time	10 min
DC power supply	QJ3005XII
Ammeter	Uni-T digital ammeter
PECE illumination	Laser diode
Post-etching treatment	Rinsed with pentane
Drying	Air stream
PSi fabrication conditions	Identical for all samples
Electrical contacts	Aluminum on both sides
Electrical characterization	Dark and illuminated I–V

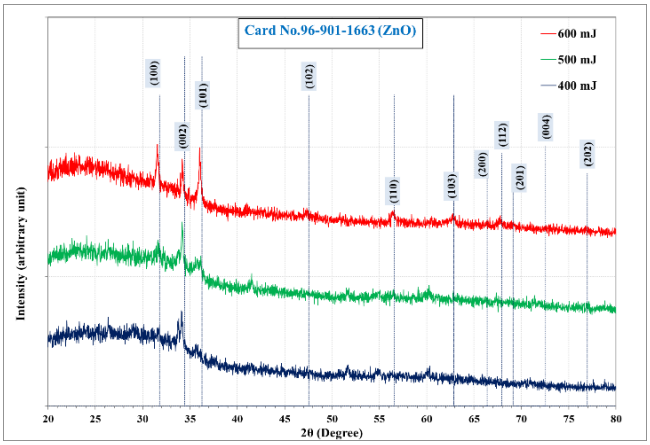

Fig. 2. ZnO film XRD patterns at various laser energies.

Among all diffraction peaks, the (002) plane exhibits the highest intensity across all samples, indicating preferred c-axis orientation [27]. This preferential orientation reflects favorable crystallinity and alignment, which are beneficial for optoelectronic applications [28]. The crystallite size (D) was calculated using the Scherrer equation [29], as follows:

$$D = \frac{0.9\lambda}{\beta \cos\theta}, \quad (1)$$

where λ is the wavelength of Cu-Kα radiation (1.5406 Å), β is the full width at half maximum (FWHM) in radians, θ is the Bragg angle, and 0.9 is the shape factor. Results show that crystallite size varies with laser energy. The (002) crystallite size is approximately 33.7 nm at 400 mJ (Table III). Lattice disruption causes the crystallite size to decrease to between 26.0 and 33.7 nm at 500 mJ, indicating a minor reduction in crystallinity. Conversely, at 600 mJ, the crystallite size recovers to a range of ~21.3 to 33.7 nm depending on the crystallographic plane, denoting superior structural ordering and enhanced grain development at higher laser power [30].

TABLE III. ZNO FILM STRUCTURAL PARAMETERS AT VARIOUS LASER ENERGIES

Energy (mJ)	2θ (Deg.)	FWHM (Deg.)	dhkl Std. (Å)	dhkl Exp. (Å)	G.S (nm)	hkl	Phase
400	34.1280	0.2466	2.6035	2.6251	33.7	(002)	Hex. ZnO
500	31.5913	0.3171	2.8137	2.8298	26.0	(100)	Hex. ZnO
	34.1985	0.2467	2.6035	2.6198	33.7	(002)	Hex. ZnO
	36.1362	0.3171	2.4754	2.4837	26.4	(101)	Hex. ZnO
600	31.5561	0.2819	2.8137	2.8329	29.3	(100)	Hex. ZnO
	34.1985	0.2466	2.6035	2.6198	33.7	(002)	Hex. ZnO
	36.0305	0.2819	2.4754	2.4907	29.6	(101)	Hex. ZnO
	56.4298	0.4228	1.6245	1.6293	21.3	(110)	Hex. ZnO
	62.8068	0.3170	1.4772	1.4783	29.4	(103)	Hex. ZnO
	67.8097	0.4227	1.3782	1.3809	22.7	(112)	Hex. ZnO

The surface structure of ZnO thin films made using the PLD method at different laser energy levels (400, 500, and 600 mJ) was examined using Atomic Force Microscopy (AFM). The 3D AFM pictures and matching height distribution histograms for the acquired films are displayed in Figs. 3, 4, and 5. AFM pictures indicate that every sample has a consistent, unbroken surface shape. Significant agglomeration and relatively bigger, irregular grain forms are visible on the surface at 400 mJ. According to research [31], [32], increasing the laser energy to 500 mJ and 600 mJ resulted in a more homogeneous and dense surface structure. The average grain size rises from 52 nm at 400 mJ to 78 nm at 500 mJ and 85 nm at 600 mJ, according to the quantitative evaluation, which is displayed in Table IV.

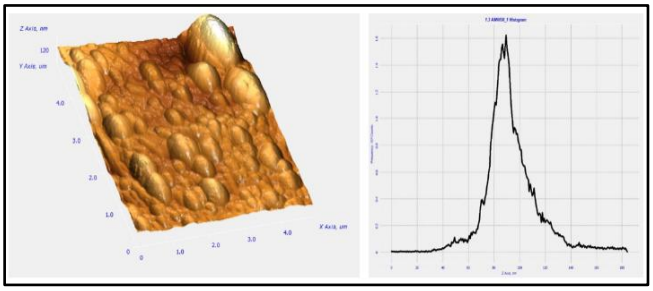

Fig. 3. AFM image for ZnO thin film at 400 mJ.

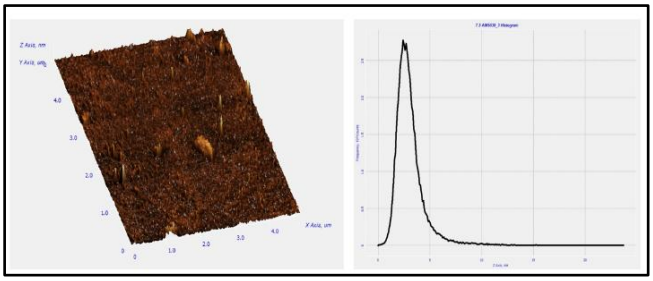

Fig. 4. AFM image for ZnO thin film at 500 mJ.

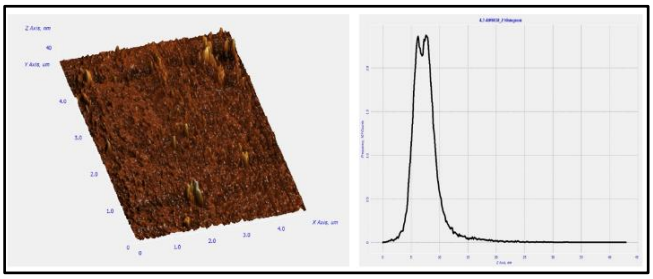

Fig. 5. AFM image for ZnO thin film at 600 mJ.

Grain enlargement and merging are facilitated by improved surface diffusion and crystallization at higher laser energy, as indicated by the rise in grain size. On the other hand, as laser energy increases, surface roughness exhibits a declining tendency. At 400 mJ, the average Ra is 3.6 nm; at 500 mJ, it is 2.5 nm; at 600 mJ, it is 1.3 nm. In a similar vein, the root mean square roughness (RMS) falls from 4.1 nm to 2.9 nm and finally to 1.5 nm. These decreases in roughness suggest that smoother and more uniform film surfaces are produced by greater laser energy [33]. The increased kinetic energy of the ablated species at higher laser energies is responsible for the observed improvement in the surface's smoothness. This improved surface mobility enables atoms to orient themselves to more energetically favorable positions, resulting in better packing and fewer surface disturbances [34].

A Scanning Electron Microscopy (SEM) technique was also used to characterize the surface structure of the ZnO thin film prepared by the PLD technique at diverse laser energies (400, 500, and 600 mJ), as shown in Fig. 6. The laser energy is 400 mJ and shows an unevenly distributed and agglomerated surface from the particles. A higher level (500 mJ) of energy gives an improved surface morphology that shows a more homogeneous distribution of particles with less aggregation. At 600 mJ, the film shows a well-distributed and dense surface, with uniformly distributed fine particles and hardly any clustering. This means that enhanced, high-quality film is obtainable under higher laser power, where a larger kinetic energy is required to move such ablated materials, which leads, in turn, to more surface diffusion, and films are thus more compact.

TABLE IV. ZNO FILM AFM CHARACTERISTICS AT VARIOUS LASER ENERGIES

Sample	Energy (mJ)	Ave. grain size (nm)	Ave. roughness (nm)	RMS (nm)
ZnO	400	52	3.6	4.1
	500	78	2.5	2.9
	600	85	1.3	1.5

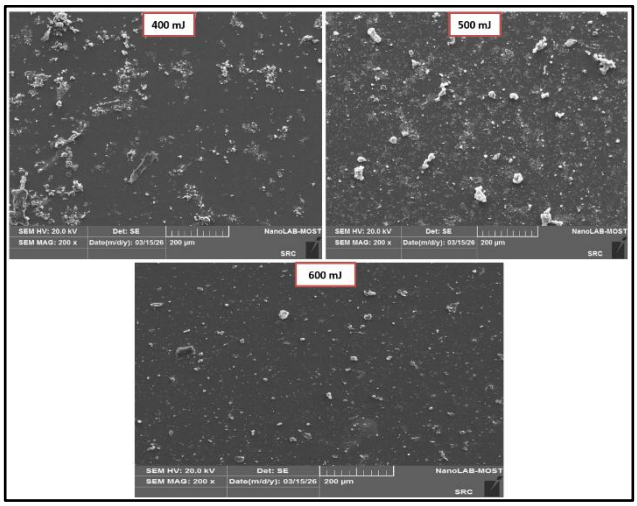

Fig. 6. SEM images of ZnO thin film at different laser energies.

In terms of the optical properties of ZnO thin films deposited using different laser energies (400, 500, and 600 mJ), UV–Vis absorption spectroscopy was used to characterize the optical characteristics. Absorbance spectra show that all the samples are extremely absorbent in the UV range (350–400 nm), but the absorbance of the visible range in the vicinity of the light and the near-infrared is decreasing progressively [35]. It is clear now to see that the greater the radiation of the laser, the lower the absorption, as in the case of the film produced at 400 mJ, and the least value obtained from the sample produced 600 mJ (Fig. 7). In contrast, transmittance spectra show an opposite trend. In addition, the transmittance rises with increasing wavelengths with higher values at visible and near-infrared regions (Fig. 8). The highest transmittance (≈85–93%) was recorded in the film produced at 600 mJ, and this was followed by the 500 mJ and 400 mJ samples. That means higher laser energy gives the films more optical clarity [36].

The relationship between absorbance (A) and transmittance (T) is expressed by [37]:

$$A = -\log(T) = \log\left(\frac{I}{I_o}\right), \quad (2)$$

where I stands for transmitted light and I_o for incoming light. The deterioration of absorbance and increase in transmittance in response to higher laser intensities may be attributed to increased crystallinity and an enhanced surface structure [38], as found in analysis using XRD and AFM. If surface imperfections and scattering points are minimized, then more light can pass through the films.

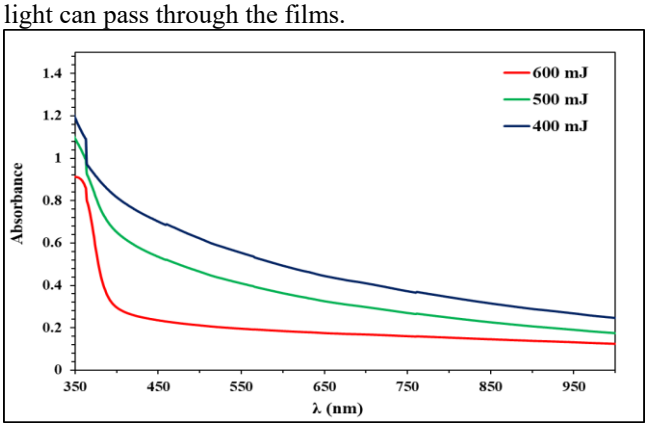

Fig. 7. Absorption of ZnO film at different laser energies

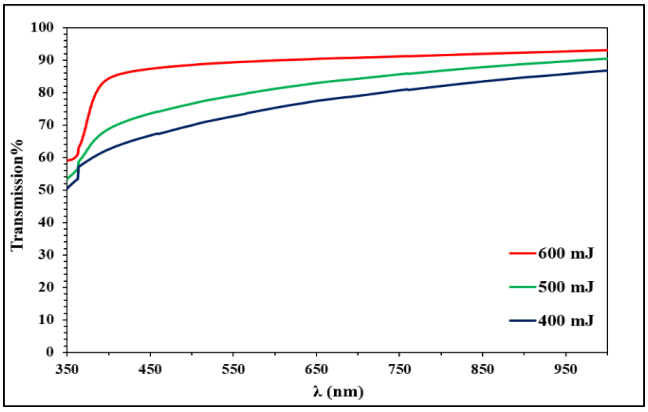

Fig. 8. Transmittance of ZnO film at different laser energies

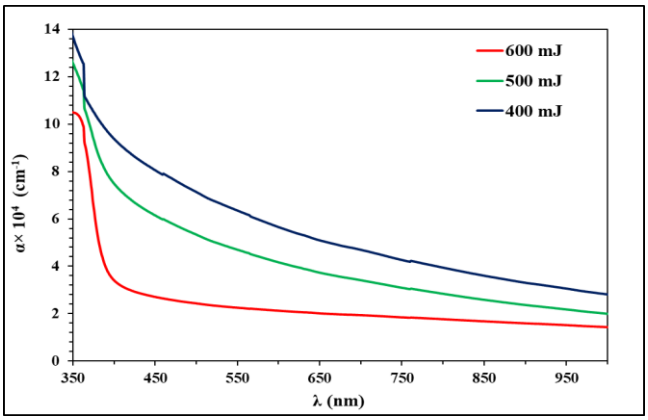

Fig. 9. α against wavelength of ZnO film at different laser energies.

A coefficient of absorption (α) for ZnO thin films deposited at 400, 500, and 600 mJ laser energies was calculated and shown in Fig. 9, which shows the decrease of the absorption coefficient with the increase of laser power across the entire wavelength range. The film fabricated at 400 mJ exhibits the maximum α, while the sample at 600 mJ shows the minimum absorption coefficient. This trend indicates that films deposited with low laser energy have a higher density of defects and greater structural disorder; therefore, they can absorb much less light [39]. The absorption coefficient increases sharply near the edge of the absorption region, which indicates strong optical transitions. The high α values (about 10^4 cm^{-1}) confirm that ZnO acts as a direct band gap semiconductor.

The absorption coefficient (α) can be determined by (3) [40]:

$$\alpha = \frac{(2.303 \times A)}{t} \quad (3)$$

t stands for the film's thickness, which is equal to 200 nm. The optical band gap Eg was determined according to the Tauc relation [41]:

$$(\alpha h\nu)^2 = A\left(h\nu - E_g\right), \quad (4)$$

where A is a constant and hν is the photon energy. It can be found that the band gap increases slightly with increasing laser energy (Fig. 10). The estimated E_g values move towards higher energies of the film treated at 600 mJ, compared to the 400 and 500 mJ films. This increase in band gap is due to increased crystallinity and decreased localized defect states in the band structure [42].

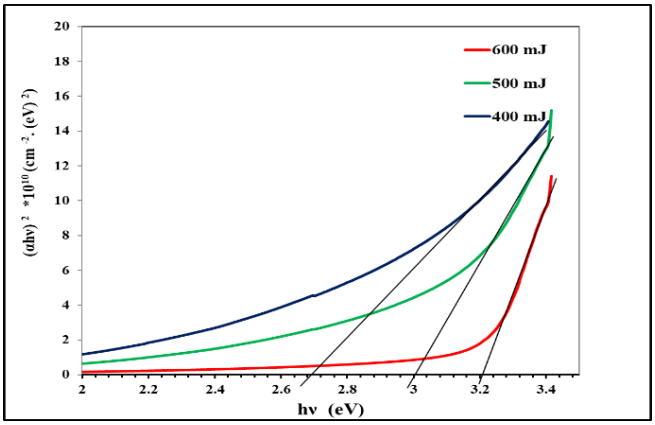

Fig. 10. $(\alpha h\nu)^2$ versus hν for ZnO film at different laser energies.

The value of the optical bandgap increased from 2.65 eV (with 400 mJ) to 2.97 eV (with 500 mJ) and reached a value of 3.19 eV with 600 mJ. The optical transmittance of the films prepared with 400 mJ, 500 mJ, and 600 mJ was measured at 950 nm, which came out to be 86.5%, 90.0%, and 92.8%, respectively. This simultaneous enhancement in both the bandgap and transmittance indicates a significant improvement in the crystalline quality of the films at higher deposition energies. The elevated energy likely reduces structural defects and localized states within the lattice, thereby minimizing optical scattering and internal absorption. Consequently, the film deposited at 600 mJ exhibits the most favorable optical properties for integration into high-efficiency optoelectronic devices.

The results of the photovoltaic analysis suggest that increasing the PLD laser energy from 400 to 600 mJ significantly enhances the efficacy of the ZnO/PSi solar cell, as shown in Fig. 11 and Table V. The maximum Voc, Jsc, Pmax, and conversion efficiency were achieved at 600 mJ, which was considered the optimal performance of the device.

This improvement is likely due to the better crystallinity, more uniform morphology, and higher optical transmittance of the ZnO film at the higher laser energy applied [43]. The fill factor (FF) showed a reduction, going down from 41.94% at 400 mJ, to 38.24% at an energy level of 500 mJ, and finally down to 36.11% at 600 mJ. Despite the increase in both the open-circuit voltage and the short-circuit current density owing to an increase in the laser energy, the reduction in the FF seems to indicate a reduction in the squareness of the J–V curves.

TABLE V. ZNO/PSI PHOTOVOLTAIC CHARACTERISTICS AT VARIOUS LASER ENERGIES.

Energy (mJ)	Voc (vol)	Jsc (mA/cm^2)	Pmax (mW/cm^2)	F.F %	h %
400	0.31	16	2.08	41.935	2.08
500	0.34	20	2.6	38.235	2.6
600	0.36	23	2.99	36.111	2.99

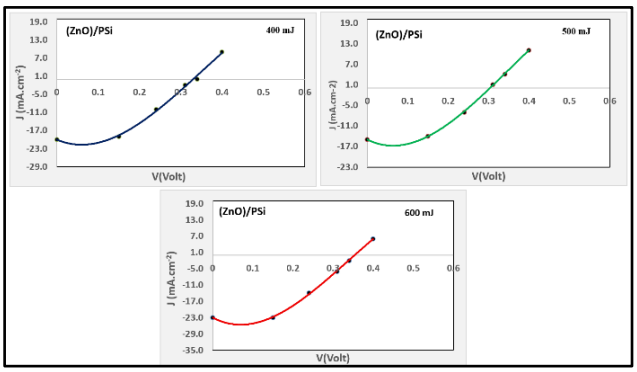

Fig. 11. J–V characteristics of ZnO/PSi at different laser energies.

IV. CONCLUSION

The results showed that increasing the laser energy is necessary to improve the quality of the films as a whole. It has been confirmed that with an increase in laser energy, crystallinity and preferred orientation improve using XRD analysis. AFM and SEM showed a better, cleaner, and more uniform surface morphology. In addition, the UV–Vis analysis results showed that optical transmittance is increased and absorption losses are reduced at high laser energies. The ZnO/PSi solar cells exhibited enhanced output power and conversion efficiency over the range of increased open-circuit voltage and short-circuit current density with higher laser energy due to these enhancements, while only showing a small decrease in fill factor value; the device demonstrated improved performance. Higher laser energy in PLD deposition is better suited to better structural conformation, better surface quality, greater optical clarity, and better photovoltaic performance. Thus, increased laser power can be considered a contributing component in maximizing ZnO thin films in the solar cell field.

REFERENCES

[1] M. A. Mimona *et al.*, "Advances and significance of nanowires in semiconductor applications," *Nano LIFE*, vol. 16, no. 3, Art. no. 2530004, 2026, doi: 10.1142/S1793984425300043.

[2] P. Phogat, R. Jha, and S. Singh, "Advanced semiconductor sensing technologies: Materials and design challenges at the nanoscale," in *Semiconductor Nanoscale Devices: Materials and Design Challenges*. Bentham Science, 2025, pp. 213–262, doi: 10.2174/9789815313208125010012.

[3] N. H. Thang and N. C. Hien, "Environmental and energy applications of green-synthesized semiconductor nanomaterials: From photocatalysis to smart sensors," *Ionics*, 2026, pp. 1–36.

[4] M. A. Issa and K. A. Aadim, "Influence of ZnO nanoparticles prepared by plasma jet and laser ablation on fungi, gram positive and gram negative bacteria," in *AIP Conf. Proc.*, vol. 3396, no. 1, Art. no. 030005, 2026, doi: 10.1063/5.0318094.

[5] S. Ghosh, D. Sarkar, S. Bastia, and Y. S. Chaudhary, "Band-structure tunability via the modulation of excitons in semiconductor nanostructures: Manifestation in photocatalytic fuel generation," *Nanoscale*, vol. 15, no. 26, pp. 10939–10974, 2023, doi: 10.1039/D3NR02116E.

[6] B. Deka, C. Baruah, A. Babu, and P. Kalita, "Biological and non-conventional synthesis of zinc oxide nanoparticles (ZnO-NPs): Their potential applications," *J. Nanotechnol. Nanomater.*, vol. 3, no. 2, pp. 79–89, 2022, doi: 10.33696/Nanotechnol.3.034.

[7] Alamgeer *et al.*, "Zinc oxide nanostructures in photovoltaics: Recent progress, technical challenges and perspectives," *Chem. Rec.*, vol. 26, no. 1, Art. no. e2500142, 2026, doi: 10.1002/tcr.202500142.

[8] P. Kumari, A. Srivastava, R. K. Sharma, D. Sharma, and S. K. Srivastava, "Zinc oxide: A fascinating material for photovoltaic applications," in *Nanomaterials for Innovative Energy Systems and Devices*. Singapore: Springer, 2022, pp. 173–241, doi: 10.1007/978-981-19-0553-7_6.

[9] Z. S. Abdul-Ridha and A. O. Radam, "Effect and study of the base temperature on the structural and optical properties of zinc oxide films prepared by thermal evaporation method in a vacuum," in *AIP Conf. Proc.*, vol. 2547, no. 1, Art. no. 030004, 2022, doi: 10.1063/5.0114795.

[10] A. Al-Rasheedi, A. R. Ansari, A. M. Abdeldaim, and M. S. Aida, "Growth of zinc oxide thin films using different precursor solutions by spray pyrolysis technique," *Eur. Phys. J. Plus*, vol. 137, no. 12, Art. no. 1371, 2022, doi: 10.1140/epjp/s13360-022-03599-2.

[11] Z. H. Azmi *et al.*, "Effect of seed layer on the growth of zinc oxide nanowires by chemical bath deposition method," *Coatings*, vol. 12, no. 4, Art. no. 474, 2022, doi: 10.3390/coatings12040474.

[12] M. A. Issa and K. A. Aadim, "Activity of (ZnO:NiO) nanoparticles prepared by plasma jet and PLD techniques against Staphylococcus aureus, Staphylococcus epidermidis, Klebsiella species, Escherichia coli and Candida albicans," in *AIP Conf. Proc.*, vol. 3415, no. 1, Art. no. 030004, 2026, doi: 10.1063/5.0322023.

[13] H. J. Seo, J. H. Yu, A. Ananth, R. H. Jeong, and J. H. Boo, "Synthesis of zinc-titanium oxide nanocomposites by plasma jet and its application to photocatalyst," *Catalysts*, vol. 12, no. 9, Art. no. 1020, 2022, doi: 10.3390/catal12091020.

[14] S. Mourad *et al.*, "Effect of oxygen annealing treatment on structural, optical and electrical properties of In doped ZnO thin films prepared by PLD technique," *Physica B*, vol. 626, Art. no. 413577, 2022, doi: 10.1016/j.physb.2021.413577.

[15] J. F. Ramos-Justicia, B. Sotillo, A. Urbieta, J. Gonzalo, and P. Fernández, "Tuning optical and electrical properties of ZnO PLD films: Effect of temperature and air annealing," *Ceram. Int.*, vol. 52, no. 1, pp. 1132–1140, 2026, doi: 10.1016/j.ceramint.2025.11.418.

[16] K. A. Aadim and M. A. Issa, "A comparative study of the optical properties of ZnO:NiO NPs synthesized by plasma jet and pulsed laser ablation: Optical properties of ZnO:NiO nano-composites," *Pak. J. Sci. Ind. Res. Ser. A: Phys. Sci.*, vol. 69, no. 2, pp. 66–72, 2026, doi: 10.52763/PJSIR.PHYS.SCI.69.2.2026.66.72.

[17] M. F. Khurshid *et al.*, "Structural, morphological, and electrical properties of zinc oxide thin films grown by pulsed laser deposition," *Phys. Solid State*, vol. 67, no. 12, pp. 1111–1119, 2025, doi: 10.1134/S1063783425602723.

[18] N. A. Bosak *et al.*, "Surface morphology, optical and electrophysical properties of cobalt-doped zinc oxide films produced by laser deposition," *J. Appl. Spectrosc.*, vol. 92, no. 6, 2026, doi: 10.1007/s10812-026-02026-z.

[19] A. A. Al-Doori and A. S. Jasim, "Characterization of zinc oxide thin film gas sensors fabricated by pulsed-laser deposition," *Iraqi J. Appl. Phys.*, vol. 21, no. 2, pp. 223–228, 2025, doi: 10.2025/gw9y3z76.

[20] M. A. Issa and K. A. Aadim, "Influence of laser energy on structural and optical properties of ZnO(x):NiO(1−x) films prepared by pulsed

laser deposition," *J. Opt.*, vol. 55, pp. 1798–1804, 2026, doi: 10.1007/s12596-024-02212-2.

[21] H. Palneedi *et al.*, "Laser irradiation of metal oxide films and nanostructures: Applications and advances," *Adv. Mater.*, vol. 30, no. 14, Art. no. 1705148, 2018, doi: 10.1002/adma.201705148.

[22] S. Chowdhury *et al.*, "Structural, morphological, and optical properties of Al-doped ZnO material synthesized via sol-gel and spin coating: Insights into crystallinity and doping effects," *Mater. Res. Bull.*, vol. 190, Art. no. 113516, 2025, doi: 10.1016/j.materresbull.2025.113516.

[23] E. Solati, L. Dejam, and D. Dorranian, "Effect of laser pulse energy and wavelength on the structure, morphology and optical properties of ZnO nanoparticles," *Opt. Laser Technol.*, vol. 58, pp. 26–32, 2014, doi: 10.1016/j.optlastec.2013.10.031.

[24] M. Arif, S. Monga, A. Sanger, P. M. Vilarinho, and A. Singh, "Investigation of structural, optical and vibrational properties of highly oriented ZnO thin film," *Vacuum*, vol. 155, pp. 662–666, 2018, doi: 10.1016/j.vacuum.2018.04.052.

[25] A. Habibi, L. Vatandoust, S. M. Aref, and H. Naghshara, "Formation of high performance nanostructured ZnO thin films as a function of annealing temperature: Structural and optical properties," *Surf. Interfaces*, vol. 21, Art. no. 100723, 2020, doi: 10.1016/j.surfin.2020.100723.

[26] N. Hacini *et al.*, "Compositional, structural, morphological, and optical properties of ZnO thin films prepared by PECVD technique," *Coatings*, vol. 11, no. 2, Art. no. 202, 2021, doi: 10.3390/coatings11020202.

[27] B. M. Nizar, M. Lajnef, J. Chaste, R. Chtourou, and E. Herth, "Highly C-oriented (002) plane ZnO nanowires synthesis," *RSC Adv.*, vol. 13, no. 22, pp. 15077–15085, 2023, doi: 10.1039/D3RA01511D.

[28] B. Li, T. Shen, and S. Yun, "Recent progress of crystal orientation engineering in halide perovskite photovoltaics," *Mater. Horiz.*, vol. 10, no. 1, pp. 13–40, 2023, doi: 10.1039/D2MH00980C.

[29] M. A. Issa and K. A. Aadim, "Optical emission spectroscopy of zinc oxide doped nickel oxide to calculate plasma parameters using the Boltzmann plot method," *Iraqi J. Phys.*, vol. 23, no. 2, pp. 118–127, 2025, doi: 10.30723/ijp.v23i2.1230.

[30] L. Zhao *et al.*, "Laser synthesis and microfabrication of micro/nanostructured materials toward energy conversion and storage," *Nano-Micro Lett.*, vol. 13, no. 1, Art. no. 49, 2021, doi: 10.1007/s40820-020-00577-0.

[31] H. Liu *et al.*, "Laser processing of flexible in-plane micro-supercapacitors: Progresses in advanced manufacturing of nanostructured electrodes," *ACS Nano*, vol. 16, no. 7, pp. 10088–10129, 2022, doi: 10.1021/acsnano.2c02812.

[32] N. Ambhore, J. E. Manikanta, N. K. Gurajala, and C. Nikhare, "Laser applications in surface treatment: A comprehensive review," *Laser Phys.*, vol. 35, no. 10, Art. no. 106101, 2025, doi: 10.1088/1555-6611/ae0df3.

[33] Y. Ding, S. Zhang, X. Luo, and J. Zhou, "AFM characterization of morphological evolution and adhesion properties of ZnO/C nanosheet-modified asphalt under UV irradiation," *Surf. Topogr.: Metrol. Prop.*, vol. 11, no. 1, Art. no. 015003, 2023, doi: 10.1088/2051-672X/acaff6.

[34] D. Park, Y. Yang, and K. Kim, "Evaluation of the mechanical properties of ZnO nanorods treated with oxygen plasma using atomic force microscopy," *Korean J. Met. Mater.*, vol. 59, no. 3, pp. 209–216, 2021, doi: 10.3365/KJMM.2021.59.3.209.

[35] S. Raha and M. Ahmaruzzaman, "ZnO nanostructured materials and their potential applications: Progress, challenges and perspectives," *Nanoscale Adv.*, vol. 4, no. 8, pp. 1868–1925, 2022, doi: 10.1039/D1NA00880C.

[36] G. M. Abdelghani, A. B. Ahmed, and A. B. Al-Zubaidi, "Synthesis, characterization, and the influence of energy of irradiation on optical properties of ZnO nanostructures," *Sci. Rep.*, vol. 12, Art. no. 20016, 2022, doi: 10.1038/s41598-022-24648-x.

[37] M. A. Issa, "Influence of Ar gas flow rate on the properties and coupling behavior of iron plasma," *Iraqi J. Appl. Phys.*, vol. 22, no. 2, pp. 317–321, 2026, doi: 10.2025/1qkzen10.

[38] F. A. Mutlak, A. F. Ahmed, U. M. Nayef, Q. Al-Zaidi, and S. K. Abdulridha, "Improvement of absorption light of laser texturing on silicon surface for optoelectronic application," *Optik*, vol. 237, Art. no. 166755, 2021, doi: 10.1016/j.ijleo.2021.166755.

[39] A. J. Haider, T. Alawsi, M. J. Haider, B. A. Taha, and H. A. Marhoon, "A comprehensive review on pulsed laser deposition technique to effective nanostructure production: Trends and challenges," *Opt. Quantum Electron.*, vol. 54, no. 8, Art. no. 488, 2022, doi: 10.1007/s11082-022-03786-6.

[40] M. A. Issa and K. A. Aadim, "Influence of gas flow rate on the plasma temperature and electron density of an atmospheric argon plasma jet," *Jordan J. Phys.*, vol. 18, no. 4, pp. 435–442, 2025, doi: 10.47011/18.4.2.

[41] M. Chitra, G. Mangamma, K. Uthayarani, N. Neelakandeswari, and E. K. Girija, "Band gap engineering in ZnO based nanocomposites," *Physica E*, vol. 119, Art. no. 113969, 2020, doi: 10.1016/j.physe.2020.113969.

[42] R. Dangi *et al.*, "Effect of oxygen vacancy on the crystallinity and optical band gap in tin oxide thin film," *Energies*, vol. 16, no. 6, Art. no. 2653, 2023, doi: 10.3390/en16062653.

[43] M. A. K. Purbayanto, A. Rusydi, and Y. Darma, "The effect of crystallinity on the surface modification and optical properties of ZnO thin films," *Phys. Chem. Chem. Phys.*, vol. 22, no. 4, pp. 2010–2018, 2020, doi: 10.1039/C9CP05464.